HHS Public Access

Author manuscript

Acta Neuropathol. Author manuscript; available in PMC 2021 February 01.

Published in final edited form as:

Acta Neuropathol. 2020 February ; 139(2): 365–382. doi:10.1007/s00401-019-02073-1.

The active contribution of OPCs to neuroinflammation is mediated by LRP1

Anthony Fernández-Castañeda[1,2], **Megan S. Chappell**[1], **Dorian A Rosen**[1,3], **Scott M. Seki**[1,2,4], **Rebecca M. Beiter**[1,2], **David M. Johanson**[1], **Delaney Liskey**[1], **Emily Farber**[5], **Suna Onengut-Gumuscu**[5], **Christopher Overall**[1], **Jeffrey L. Dupree**[6], **Alban Gaultier**[1,#]

[1]Center for Brain Immunology and Glia, Department of Neuroscience, School of Medicine, University of Virginia, Charlottesville, VA, 22908, USA.

[2]Graduate Program in Neuroscience, School of Medicine, University of Virginia, Charlottesville, VA, 22908, USA.

[3]Graduate Program in Pharmacological Sciences, School of Medicine, University of Virginia, Charlottesville, VA, 22908, USA.

[4]Medical Scientist Training Program, School of Medicine, University of Virginia, Charlottesville, VA, 22908, USA.

[5]Center for Public Health Genomics, School of Medicine, University of Virginia, Charlottesville, VA, 22908, USA.

[6]Department of Anatomy and Neurobiology, Virginia Commonwealth University, Richmond, Virginia 23298, USA.

Abstract

Oligodendrocyte progenitor cells (OPCs) account for about 5% of total brain and spinal cord cells, giving rise to myelinating oligodendrocytes that provide electrical insulation to neurons of the CNS. OPCs have also recently been shown to regulate inflammatory responses and glial scar formation, suggesting functions that extend beyond myelination. Low-density lipoprotein related-receptor-1 (LRP1) is a multi-faceted phagocytic receptor that is highly expressed in several CNS cell types, including OPCs. Here, we have generated an oligodendroglia-specific knockout of LRP1, which presents with normal myelin development, but is associated with a better outcome in two animal models of demyelination (EAE and cuprizone). At a mechanistic level, LRP1 did not directly affect OPC differentiation into mature oligodendrocytes. Instead, animals lacking LRP1 in OPCs in the demyelinating CNS were characterized by a robust dampening of inflammation. In particular, LRP1-deficient OPCs presented with impaired antigen cross-presentation machinery, suggesting a failure to propagate the inflammatory response and thus promoting faster myelin

[#]**Corresponding author:** ag7h@virginia.edu.

repair and neuroprotection. Our study places OPCs as major regulators of neuroinflammation in an LRP1-dependent fashion.

INTRODUCTION

Chronic demyelination is the major reason for disease progression and increased disability in multiple sclerosis (MS) patients, as exposed neurons are prone to neurodegeneration [36]. Understanding the mechanisms of remyelination is critical in preventing neuronal loss, and is paramount to improving the quality of life of MS patients [23]. The adult CNS contains a large population of oligodendrocyte progenitor cells (OPCs) that have the potential to differentiate into mature oligodendrocytes and remyelinate denuded axons [23]. Despite OPCs being efficiently recruited into MS lesions [13], the process of axon remyelination is impaired [42]. A multitude of factors in MS plaques inhibit OPC differentiation into mature oligodendrocytes, including myelin debris, the glial scar, and cytotoxic inflammation [4, 10, 12, 41, 43].

Beyond their role in myelination, OPCs have now been shown to be active players in CNS pathology. OPCs, similar to microglia, are constantly surveilling their environment and can migrate to sites of CNS injury [34]. In mouse models of MS, OPCs can upregulate cytokine production in response to IL-17 signaling, and greatly contribute to CNS pathogenesis [37]. Surprisingly, OPCs also upregulate antigen presentation machinery in the demyelinating CNS, and can regulate CD4 T cell proliferation and survival *in vitro* [19]. Additionally, OPCs can cross-present antigen via MHC1 and activate CD8 T cells, further shaping the inflammatory milieu [39]. Taken together, these studies highlight the dynamic role OPCs play in the diseased CNS.

Low-density lipoprotein receptor-related protein 1 (LRP1) is a member of the LDL receptor gene family that functions in receptor-mediated endocytosis and cell signaling [44]. With regards to white matter repair, LRP1 is known to be expressed by the oligodendrocyte lineage [3] and to function as a phagocytic receptor for myelin debris [21, 26]. The phagocytic properties of LRP1 have also been shown to greatly influence extracellular matrix remodeling and expression of matrix metalloproteinases [25, 59]. Additionally, LRP1 has a central role in inflammation due to its ability to regulate cytokine production [9, 24, 48, 61]. LRP1 has also been shown to play a role in dendritic cell efferocytosis and MHC1-dependent antigen cross-presentation [60]. Taken together this evidence places LRP1 as a potential key player in the context of remyelination, but the contribution of LRP1 in OPCs during neuroinflammation remains unclear.

Herein, we report LRP1 expression in OPCs in adult mice and human oligodendroglia. Using two animal strains lacking LRP1 in the oligodendrocyte lineage, we show that the inflammatory environment was significantly dampened in LRP1-deficient mice, resulting in neuroprotection and enhanced myelin regeneration in the Experimental Autoimmune Encephalomyelitis (EAE) and cuprizone models, respectively. Mechanistically, we show that LRP1-deficient OPCs have no intrinsic defect involved in their differentiation into mature oligodendrocytes but have impaired MHC1-dependent antigen cross-presentation, which could explain the enhanced neuroprotection and remyelination.

RESULTS

Cells of the oligodendrocyte lineage dynamically express LRP1

LRP1 expression in the CNS is differentially regulated during development, with glial cells and, in particular, OPCs expressing high levels of LRP1 into adulthood. Oligodendrocytes and myelin are not reported to express LRP1 in the adult CNS [3, 26, 63]. Indeed, the majority of PDGFRα$^+$ OPCs in the corpus callosum expressed LRP1 (Fig. 1a,b, arrows, 97.5%), while only a small percentage of CC1$^+$ oligodendrocytes (Fig. 1a,b, dented arrowheads, 7.6%) were LRP1 positive. Additional staining for LRP1 performed on *Mobp*-EGFP mice [29] revealed that GFP$^+$ cells are LRP1 negative (Fig. S1b), suggesting that LRP1 expression might be progressively lost during OPC differentiation into oligodendrocytes, a result consistent with published results [63]. To analyze whether human OPCs also express LRP1, we tested postmortem human white matter Olig2$^+$ cells, and discovered that a subset of these cells also expressed LRP1 and had typical OPC morphology (Fig. 1c). Furthermore, we also detected LRP1 expression in OPCs during pathological conditions. We found PDGFRα$^+$ Olig2$^+$ LRP1$^+$ OPCs in tissue isolated from mice undergoing cuprizone-mediated demyelination and EAE (Fig. 1d,e). Taken together, our results confirm and highlight LRP1 expression in human and murine adult OPCs during homeostatic and pathological conditions.

Myelin homeostasis is normal in animals lacking LRP1 in oligodendrocyte lineage

To study the function of LRP1 in the oligodendrocyte lineage *in vivo*, we crossed *Lrp1*$^{fl/fl}$ animals with mice expressing Cre recombinase under the *Olig1* promoter [47]. *Lrp1*$^{fl/fl}$*Olig1*^{Cre} and *Olig1*^{Cre} (Cre-expressing wild type) mice were born according to Mendelian ratios, and appeared healthy and fertile. As expected, LRP1 expression was undetectable by immunofluorescence in PDGFRα$^+$ OPCs in the *corpus callosum* of adult *Lrp1*$^{fl/fl}$*Olig1*^{Cre} mice, but remained detectable in NeuN$^+$ cortical neurons (Fig. 2a, Fig. S2c). LRP1 transcript and protein were not detected in purified primary OPCs isolated from *Lrp1*$^{fl/fl}$*Olig1*^{Cre} mice (Fig. S2a,b). As a control, we also performed IBA1 staining in adult brains to visualize microglia, the resident immune cells in the CNS, and found that deletion of LRP1 in OPCs did not result in perturbation of microglial number or morphology (Fig. S2c). These findings confirmed specific deletion of LRP1 in OPCs in our model. To address whether deletion of LRP1 in OPCs was associated with a myelination defect, we began by quantifying myelin protein expression in adult mice (5 months old). Protein extracts were prepared from the cerebrum and cerebellum of *Lrp1*$^{fl/fl}$*Olig1*^{Cre} and control *Olig1*^{Cre} mice and expression of MBP and CNP was analyzed via immunoblot. In the cerebellum, CNP and MBP expression was similar across genotypes, whereas the cerebrum of *Lrp1*$^{fl/fl}$*Olig1*^{Cre} mice had a modest but statistically significant decrease in MBP and CNP expression (Fig. 2b–d). To further analyze the contribution of LRP1 in myelination, optic nerves from 8-week old *Lrp1*$^{fl/fl}$*Olig1*^{Cre} and *Olig1*^{Cre} mice were prepared for transmission electron microscopy (TEM) analysis of myelin ultrastructure and determination of the *g*-ratio (Fig. 2e). Linear fitting of the *g*-ratio data showed no differences between the two groups of mice (Fig. 2f). Taken together, our results show that overall myelin structure in adult mice appears normal following specific deletion of LRP1 in OPCs, with a modest decrease in MBP and CNP expression that is unique to the cerebrum.

Enhanced OPC differentiation in LRP1-deficient mice after cuprizone-induced demyelination

Since LRP1 has been shown to regulate pathological conditions applicable to demyelination, such as the inflammatory response and the removal of myelin debris [20, 24, 26], we subjected our mice to a pathological model of demyelination: the cuprizone model. Cuprizone is a copper chelator that induces reversible demyelination in the *corpus callosum* by inducing selective oligodendrocyte apoptosis [27, 38]. Once the animals are returned to their regular diet, OPCs differentiate and remyelination in the *corpus callosum* occurs. Mice were fed a 0.3% cuprizone diet for 5 weeks and then returned to a normal diet to allow for remyelination in the CNS (Fig. 3a). We quantified OPC ($Olig2^+$ $PDGFR\alpha^+$) and oligodendrocyte ($Olig2^+$ $CC1^+$) numbers in the *corpus callosum* during homeostatic conditions, peak demyelination, or two remyelination stages, as indicated in Fig. 3a **(left panel)**. Under homeostasis, we found no differences in the number of OPCs or mature oligodendrocytes in the *corpus callosum* of $Lrp1^{fl/fl}Olig1^{Cre}$ and $Olig1^{Cre}$ mice (Fig. 3c,e, **Unt;** Fig. S3b,c). This is in agreement with our data suggesting no major defects in myelination in LRP1-knockout animals (Fig. 2). $Lrp1^{fl/fl}Olig1^{Cre}$ mice also experienced similar oligodendrocyte loss and comparable OPC expansion at the peak of cuprizone-induced demyelination (Fig. 3c,e, **Dem;** Fig. S3d,e). Notably, the loss of mature oligodendrocytes correlated with an equal decrease in MBP expression in the *corpus callosum* (Fig. S4a). The number of $Ki67^+$ OPCs or total $Ki67^+$ cells between genotypes at the peak of demyelination was comparable, which indicated that deletion of LRP1 does not affect OPC proliferation (Fig. 3f–h). Surprisingly, we noted a significant increase in the oligodendrocyte numbers in $Lrp1^{fl/fl}Olig1^{Cre}$ mice, compared to $Olig1^{Cre}$ controls at both remyelination time points examined (Fig. 3b,c, **0.5 and 1 Wk Rem**). This increase in oligodendrocytes correlated with a significant decrease in the number of OPCs (Fig. 3d,e, **0.5 Wk Rem**), suggesting enhanced OPC differentiation in the absence of LRP1. Overall, our data suggest that deletion of LRP1 in OPCs enhances OPC differentiation into oligodendrocytes following cuprizone-induced demyelination. To explore if the increase in oligodendrocyte numbers in $Lrp1^{fl/fl}Olig1^{Cre}$ mice translates into increased myelin synthesis, we analyzed MBP expression on coronal brain sections by immunofluorescence. We saw a significant increase in MBP coverage in $Lrp1^{fl/fl}Olig1^{Cre}$ mice (Fig. 4a,b). We also analyzed myelin ultrastructure in the *corpus callosum* of $Lrp1^{fl/fl}Olig1^{Cre}$ mice by TEM and observed a trend towards a higher percentage of myelinated axons (Fig. 4c,d). No difference in myelin *g*-ratios was observed between the genotypes (Fig. S4b). Collectively, these results indicate that deletion of LRP1 in OPCs accelerates myelin repair after cuprizone-induced demyelination.

Oligodendrocyte maturation *in vitro* does not require LRP1 expression in OPCs

To determine whether enhanced remyelination in LRP1-deficient mice was cell-intrinsic, we isolated primary OPCs from $Lrp1^{fl/fl}Olig1^{Cre}$ and $Olig1^{Cre}$ neonate (post-natal day 8) animals and induced their differentiation into myelinating oligodendrocytes with triiodothyronine (T3) for 48 hours [18]. We then analyzed expression of myelin genes *Mrf*, *Mbp*, and *Cnp* by qPCR. To our surprise, we found no significant differences between $Lrp1^{fl/fl}Olig1^{Cre}$ and $Olig1^{Cre}$ OPCs (Fig. 4e–g). Additionally, when cultured OPCs derived

from *Plp*-EGFP reporter mice were cultured in the absence of T3 and treated with increasing concentrations of receptor-associated protein (RAP), an LRP1 antagonist that blocks ligand binding to LRP1 [33], we found no differences in the percent of *Plp*-EGFP positive cells, compared to vehicle control (Fig. 4h,i). These data suggest that enhanced OPC differentiation in $Lrp1^{fl/fl}Olig1^{Cre}$ mice after cuprizone treatment is not likely to be mediated by a cell-intrinsic mechanism in OPCs.

Oligodendroglial LRP1 regulates the inflammatory environment and promotes myelin repair

Given the unexpected lack of a cell-autonomous differentiation phenotype in $Lrp1^{fl/fl}Olig1^{Cre}$ OPCs *in vitro*, and the fact that naïve $Lrp1^{fl/fl}Olig1^{Cre}$ mice have similar numbers of OPCs and oligodendrocytes in the *corpus callosum*, we postulated that OPCs lacking LRP1 could influence the local environment to promote remyelination via an indirect mechanism under pathological demyelination. To test this, we performed unbiased RNA-sequencing analysis on micro-dissected *corpus callosum* from homeostatic or remyelinating mice post-cuprizone treatment (Fig. 5a). Principal component analysis (PCA) revealed that $Lrp1^{fl/fl}Olig1^{Cre}$ and $Olig1^{Cre}$ *corpus callosum* samples under homeostatic conditions were comparable (Fig. 5b). However, striking gene expression differences between the remyelinating *corpus callosum* of $Lrp1^{fl/fl}Olig1^{Cre}$ and $Olig1^{Cre}$ mice were detected (Fig. 5c,d). Gene ontology (GO) terms associated with myelination and oligodendrocyte differentiation were elevated in $Lrp1^{fl/fl}Olig1^{Cre}$ mice (Fig. 5e), supporting our histological analysis (Fig. 4). Indeed, prototypical genes involved in myelination (*Cnp*, *Mbp*, *Plp1*) were significantly elevated in in the *corpus callosum* of $Lrp1^{fl/fl}Olig1^{Cre}$ mice (Fig. 5f). Surprisingly, $Lrp1^{fl/fl}Olig1^{Cre}$ mice also had a dampened inflammatory signature, compared to $Olig1^{Cre}$ mice (Fig. 5g). The change in the inflammatory response was detectable at week 5 (Fig. S5c), a stage preceding remyelination [58] (Fig. S5b), without an overall change in IBA1 immunoreactivity (Fig. S5d,e). Collectively, our data suggest that LRP1 expression in OPCs might modulate the immune landscape in the cuprizone model.

LRP1 deletion in OPCs is protective in experimental autoimmune encephalomyelitis

The unexpected role of LRP1 in OPCs as a regulator of the inflammatory response in the cuprizone model of demyelination prompted us to further explore OPC LRP1 function in neuroinflammation. For this, we chose experimental autoimmune encephalomyelitis (EAE), a well-accepted model of the neuroinflammatory human disease multiple sclerosis (MS). We tested $Lrp1^{fl/fl}Olig1^{Cre}$ and control $Olig1^{Cre}$ mice in EAE, and found reduced clinical scores and delayed incidence of disease onset in $Lrp1^{fl/fl}Olig1^{Cre}$ mice, compared to control mice (Fig. 6a,b). This phenotype was recapitulated with an alternate inducible model of LRP1 deletion in OPCs ($Lrp1^{fl/fl}Pdgfra^{CreERt2}$). In this model, mice were injected with tamoxifen (to induce LRP1 deletion) at 8 weeks of age, followed by EAE immunization 4 weeks later. Tamoxifen is known to inhibit inflammation explaining the milder EAE clinical score and incidence obtained with this inducible Cre strain [6], nevertheless LRP1 deletion also resulted in a significant decrease in clinical score (Fig. S6a). To explore the pathological conditions associated with lower EAE clinical scores in $Lrp1^{fl/fl}Olig1^{Cre}$ mice, we performed flow cytometry analysis at the peak of the disease (day 17). Our results reveal that the numbers of $TCR\beta^+$ T cells ($TCR\beta^+$ $CD8^-$), CD8 T cells ($TCR\beta^+$ $CD8^+$), and myeloid

cells ($CD11b^+$ $CD45^+$) were decreased in animals lacking LRP1 expression in OPCs, compared to control mice (Fig. 6c–f). T regulatory cell ($TCR\beta^+$ $CD4^+$ $FoxP3^+$) numbers were equivalent in the spinal cord and the draining inguinal lymph nodes across genotypes during EAE (Fig. S6b). Importantly, the number of OPCs ($CD45^-$ $PDGFR\alpha^+$) was similar across genotypes (Fig. 6g–i).

To rule out immune dysfunction in *Lrp1*$^{fl/fl}$*Olig1*^{Cre} mice as the driver of our immunomodulatory phenotype, we tested the antigen recall response of lymph node T cells 7 days after immunization. Treatment with the $MOG_{35–55}$ peptide resulted in a mild increase in IFNγ without significant differences in the production of IL-17A, as determined by multiplex immunoassay (Fig. 6j,k). Importantly, analysis of the spleen 7 days post-immunization did not reveal differences in T cell numbers (Fig. S6c), ruling out an LRP1-dependent defect in immunization as the origin of our phenotype. EAE resistance was not due to the baseline differences in immune cell composition, as demonstrated by immunophenotyping analysis of the immune organs of *Lrp1*$^{fl/fl}$*Olig1*^{Cre} and *Olig1*^{Cre} animals under homeostatic conditions (cervical lymph nodes and spleen; Fig. S6d–f). One exception being a small decrease in the frequency of CD8+ T cells in naïve spleens of *Lrp1*$^{fl/fl}$*Olig1*^{Cre}. Taken together, our results show that mice lacking LRP1 expression in OPCs have reduced inflammation in EAE, paralleling our results obtained with the cuprizone model.

LRP1 regulates antigen cross-presentation by OPCs

Recently, OPCs have been shown to cross-present antigen via MHC1 in demyelinating conditions [39]. Antigen cross-presentation was of particular interest because of the documented role of LRP1 in internalizing antigenic stimuli that is processed and presented to CD8 T cells via MHC1 [5, 8, 32, 60]. We began by measuring the expression of MHC1 at the peak of EAE in *Lrp1*$^{fl/fl}$*Olig1*^{Cre} and *Olig1*^{Cre} mice and found that LRP1-deficient OPCs have significantly lower levels of MHC1 (Fig. 7a,b). We next examined myeloid cells ($CD45^+$ $CD11b^+$) and detected two populations based on MHC1 expression ($MHC1^{Mid}$ and $MHC1^{High}$, Fig. 7c–e). Backgating showed that $MHC1^{High}$ cells are $CD45^{High}$ $CD11b^+$ and that $MHC1^{Mid}$ cells are $CD45^{Mid}$ $CD11b^+$ (Fig. 7f); an expression pattern that has been used to loosely classify microglia and invading myeloid cells [17]. Our results suggest that MHC1 expression does not change in $CD45^{Mid}$ $CD11b^+$ $MHC1^{Mid}$ (microglia, Fig. 7d) but is decreased in $CD45^{High}$ $CD11b^+$ $MHC1^{High}$ (peripheral myeloid cells, Fig. 7e). We then decided to isolate OPCs and myeloid cells from EAE spinal cords to further explore antigen cross-presentation defects in LRP1-deficient OPCs and the consequences on the inflammatory environment (Fig. S7a,b). The labeling strategy for cell sorting was designed to eliminate contaminating endothelial cells ($CD31^+$) and pericytes ($CD13^+$) that are known to also express PDGFRα (Fig. 7g). RNA-sequencing analysis revealed decreased expression of antigen cross-presentation machinery, including MHC1, in OPCs ($PDGFR\alpha^+$) lacking LRP1 (Fig. 7h). Excitingly, decreased MHC1-related gene expression was conserved in our cuprizone model RNA-sequencing dataset (Fig. 7i). Because myeloid cells are critical orchestrators of demyelination [1, 28], we also analyzed gene expression in isolated myeloid cells ($CD11b^+$ $CD45^+$) from the spinal cord of *Lrp1*$^{fl/fl}$*Olig1*^{Cre} and *Olig1*^{Cre} mice subjected to EAE. We found that the inflammatory response to IFNγ, a cytokine produced by antigen-

stimulated CD8 and CD4 T cells, was robustly elevated in myeloid cells from *Olig1*^{Cre} mice, when compared to the cells from *Lrp1*$^{fl/fl}$*Olig1*^{Cre} mice (Fig. 7j). This observation also phenocopied our cuprizone results, as IFNγ response genes were also decreased in remyelinating *corpus callosum* of *Lrp1*$^{fl/fl}$*Olig1*^{Cre} mice (*Nos2, Ccl5, Nlrc5*; Fig. 5g). We next quantified CD8 T cells present in the brain of cuprizone-fed mice, and EAE spinal cords and did not detect any significant changes between genotypes (Fig. S8a,b,d,e). However, the number of CD8 T cells associating with OPCs (Fig. 7k) was trending lower in the cuprizone and EAE models in *Lrp1*$^{fl/fl}$*Olig1*^{Cre} mice (Fig. S8 c,f). To assess the role of LRP1 in antigen cross-presentation, we treated primary OPCs with IFNγ to induce MHC1 expression [40]. OPCs were then incubated with ovalbumin (OVA) protein in the presence or absence of RAP, an LRP1 inhibitor [33]. After a media wash, OPCs were cocultured with OT-I CD8 T cells (OVA-specific) for 48h. Finally, CD8 T cell proliferation was quantified by flow cytometry. Our results show that blocking LRP1 with RAP is able to significantly decrease CD8 T cell proliferation *in vitro* (Fig. 7l). Taken together, our results suggest that LRP1 deletion in OPCs may disrupt antigen cross-presentation to lymphocytes and thus could influence the function of T cells and myeloid cells in the demyelinating CNS.

DISCUSSION

Understanding the mechanisms that control neuroinflammation and promote neuroprotection in MS is paramount for the development of critically needed therapeutics. Here, we have presented evidence further highlighting the role of OPCs in actively shaping the neuroinflammatory landscape. Using two distinct models of demyelination, we have shown that the immunomodulatory function of OPCs relies on the multifunctional receptor LRP1. The specific removal of LRP1 in OPCs (*Lrp1*$^{fl/fl}$*Olig1*^{Cre} or *Lrp1*$^{fl/fl}$*Pdgfra*^{CreERt2} mice) reduces the inflammatory response during CNS demyelination and promotes repair and neuroprotection.

Intriguingly, in our hands, *Lrp1*$^{fl/fl}$*Olig1*^{Cre} mice appear to have unperturbed developmental myelination, in contrast with a recent study that utilized *Olig2*-Cre mediated deletion of LRP1 [45]. We did not observe myelin ultrastructure abnormalities in adult *Lrp1*$^{fl/fl}$*Olig1*^{Cre} animals, though we noted modestly decreased MBP and CNP expression in the cerebrum of these mice. There are several possible explanations for the observed differences in the role of LRP1 in developmental myelination between our study and Lin *et al* [45]. One, it is possible that a transient myelination deficit exists in *Lrp1*$^{fl/fl}$*Olig1*^{Cre} mice at earlier developmental time points, which is not apparent in the adult animals we examined. The slight decrease in MBP and CNP expression detected in the cerebellum, but not present in the cerebrum, could be linked to the significant difference in myelin quantity between these two CNS regions. Perhaps, a mild developmental myelin defect is only detectable in heavily myelinated areas in our strain, but the role of LRP1 in pathological inflammatory conditions (antigen cross-presentation) outweighs this mild phenotype. Furthermore, we did not observe differences in the *in vitro* differentiation of OPCs (isolated from newborn mice) after either genetic or pharmaceutical inactivation of LRP1. Second, our mouse model employs the use of the *Olig1*-Cre knock-in allele [47]. Because *Olig1* deficiency has been reported to cause remyelination and developmental myelination deficits [2, 16], we utilized *Olig1*^{Cre} animals as controls for *Lrp1*$^{fl/fl}$*Olig1*^{Cre} mice (in order to minimize any differences due to the

inactivation of one *Olig1* allele). Such consideration could perhaps mask the subtle LRP1-dependent phenotype observed during myelin formation by Lin *et al.* [45]. Third, there are fundamental differences in the models selected for our study - cuprizone and EAE are associated with extensive demyelination and induction of immune responses, compared to the focal lysolecithin demyelination model used by Lin *et al.* [54].

In this study we demonstrate that the removal of LRP1 in OPCs is associated with a better outcome in animal models of demyelination (cuprizone and EAE). This improvement was not due to a direct effect on the differentiation of OPCs into oligodendrocytes, but was mediated by modulation of the inflammatory environment. Specifically, we observe a downregulation of genes involved in MHC1 antigen cross-presentation in LRP1-deficient OPCs. Additionally, the CNS of these mice also presents with a dampened inflammatory profile. Our results are consistent with a previous study that shows wild type OPCs upregulate antigen cross-presentation machinery in the demyelinating CNS [19]. LRP1 blockade or genetic deletion has been shown to prevent antigen presenting cells from engulfing exogenous peptides or apoptotic cells, thereby negatively affecting MHC1-mediated cross-presentation [7, 8, 60]. We propose OPCs internalize antigen in an LRP1-dependent fashion, which is then processed and cross-presented to CD8 T cells during CNS demyelination (Fig. 8). CD8 T cells can then engage in a multitude of effector functions to exacerbate CNS pathology, for example production of perforin and granzyme B, or secretion of IFNγ and TNFα [62]. It has been well documented that IFNγ and TNFα can stunt OPC differentiation [14, 46]. Furthermore, CD8-derived IFNγ plays a crucial role in EAE pathogenesis, specifically in models where oligodendrocytes are engineered to cross-present antigen to CD8 lymphocytes [22, 35, 51, 52]. Indeed, we observed a downregulation of cross-presentation machinery in LRP1-deficient OPCs, which is accompanied by decreased expression of IFNγ-related genes in the CNS (Fig. 5g; Fig. 7h). Another possible explanation for our results is the potential role of LRP1 on cell migration [44]. Perhaps, LRP1-deficient OPCs migrate faster to the site of remyelination from adjacent regions of the parenchyma or stem cell niches to accelerate myelin repair [11].

Our results are in agreement with recent work showing that OPCs can participate in antigen-cross presentation and activate CD8 T cell effector functions, leading to impaired myelin repair in the cuprizone model [39]. Future studies will be critical to understand if LRP1 is needed to mediate CD8 T cell cytotoxicity toward OPCs in the context of MS and to identify the antigens involved in this pathological process. Other studies are also needed to determine if the change of the inflammatory environment is downstream of CD8 T cells or an independent arm of LRP1 function in OPCs. Clearly, LRP1 in OPCs might also influence other immune cells such as CD4 and myeloid cells in the context of demyelination; further work is needed to tease apart the effect of LRP1 in OPCs on different inflammatory cell types.

Based on our results, targeting LRP1 in the context of MS appears to be an attractive therapeutic intervention, but caution should be taken due to the pleiotropic and multifunctional nature of LRP1 [30]. Other cells in the CNS, such as microglia and neurons, express LRP1 and LRP1 function can vary greatly across cell types [44]. LRP1 deletion in microglia results in higher pro-inflammatory cytokines and increased EAE severity [15].

This phenotype is mediated in part by increased NF-κB activity [15]. Yet, abrogating NF-κB signaling in oligodendroglia does not mirror the findings presented here [53], strengthening the point that other LRP1-dependent mechanism(s) are at play in our system. Furthermore, LRP1 deletion in neurons has been reported to be associated with motor dysfunction, likely due to impaired neurotransmission [50]. While the precise targeting of LRP1 in OPCs might be technically challenging, future studies are needed to determine upstream and downstream pathways associated with LRP1 to discover OPC-based treatments to promote remyelination and neuroprotection.

METHODS

Human subjects

Fresh frozen brain tissues from multiple sclerosis patients with pathological evaluations were obtained from the Rocky Mountain MS center Brain Bank.

Animals

Mice in the C57BL/6J background with loxP sites flanking the *LRP1* gene (Jackson #012604) were crossed with $Olig1^{Cre/Cre}$ (Jackson #011105) or $Pdgfra^{Cre\text{-}ERt2}$ (Jackson #018280) mice to generate $Lrp1^{fl/fl}Olig1^{Cre}$ mice and $Lrp1^{fl/fl}Pdgfra^{Cre\text{-}ERt2}$. $Olig1^{Cre}$ mice were used as a negative control across all the studies when using $Lrp1^{fl/fl}Olig1^{Cre}$ mice. $Lrp1^{fl/fl}Pdgfra^{Cre\text{-}ERt2-}$ mice were used as negative controls when studying $Lrp1^{fl/fl}Pdgfra^{Cre\text{-}ERt2+}$ mice. Mice were maintained in the C57BL/6J background by performing backcrossing every 2–3 generations. OT-I mice were purchased from Jackson (#003831). *Mobp*-EGFP mice were purchased from MMRRC (#030483-UCD). The age of experimental animals is indicated in Table S1. All animal experiments were approved and complied with regulations of the Institutional Animal Care and Use Committee at University of Virginia (#3918).

Reagents

Primary antibodies used for immunofluorescence were against LRP1 (ab92544, 1:5000, Abcam), PDGFRα (AF1062, 1:200, R&D Systems), CC1 (OP80, 1:200, Millipore), Olig2 (AB9610, 1:500, Millipore), Olig2 (MABN50, 1:500, Millipore), MBP (ab7349, 1:500, Abcam), CD8 (14–0081-82, 1:200, eBioscience), and Ki67 (ab15580, 1:300, Abcam). Primary antibodies used for immunoblotting were against LRP1 (L2170, 1:1000, Sigma), MBP (SMI-94, 1:1000, Covance), CNP (CNP, 1:2000, Aves Labs), actin (A2228, 1:5000, Sigma). GST-RAP was expressed in bacteria and purified as previously described [33].

Animal models of demyelination

For the cuprizone model, adult male mice (ages in Table S1) were fed regular chow mixed with 0.3% cuprizone (Sigma #14690) ad libitum for 5 weeks to induce demyelination as previously described [55]. For EAE, $Lrp1^{fl/fl}Olig1^{Cre}$ and $Olig1^{Cre}$ mice were immunized and scored as previously described [57].

Tamoxifen (T5648, Sigma) was prepared at 20mg/mL in 0.2μm filtered corn oil (C8267, Sigma) by shaking overnight at 37°C. $Lrp1^{fl/fl}Pdgfra^{Cre\text{-}ERt2}$ adult mice received two IP

injections of 200mg/kg tamoxifen, two days apart. No more than 4mg tamoxifen per injection was administered to adult mice. Mice were allowed to recover for 4 weeks after the final tamoxifen injection before EAE immunizations. *Lrp1fl/flPdgfraCre-ERt2−* and *LRP1fl/flPdgfraCre-ERt2+* mice were immunized twice, three weeks apart, due to the immunomodulatory effects of tamoxifen [6, 31]. EAE scores for $Lrp1^{fl/fl}Pdgfra^{Cre\text{-}ERt2}$ mice were collected after the second immunization.

Immunofluorescence and transmission electron microscopy

Mice were euthanized and perfused with PBS containing 5U/mL heparin followed by 10% buffered formalin. Tissue was post-fixed at least 24h and allowed to sink in 20% sucrose at 4°C. Free-floating cryosections were cut (30–40μm) and collected in PBS containing 0.02% sodium azide and stored at 4°C until further analysis. Sections were blocked in PBS, 0.3% Triton-X 100, 1% BSA, 2% serum for at least 2h at room temperature. When using mouse antibodies on mouse tissue, M.O.M Blocking Reagent (Vector Labs) was also used for 1h at room temperature. Sections were then placed in primary antibody cocktail overnight at 4°C. Tissue was washed three times in PBS, incubated in corresponding secondary antibodies at 2μg/mL (Jackson Immuno Research), and counterstained with Hoechst. Sections were mounted using Aqua-Mount (Lerner Labs) mounting medium, imaged using a Leica TCS SP8 confocal microscope, and analyzed in Imaris (Bitplane) or Fiji [56]. Mouse tissue was prepared for transmission electron microscopy as previously described [49]. Fresh-frozen human tissue samples were acquired from the Rocky Mountain MS Center Tissue Bank at the University of Colorado.

Immunoblot

Cerebrum and cerebellum protein were extracted in RIPA buffer with cOmplete Protease Inhibitor Cocktail (Roche). Lysates were centrifuged (13,000 × g, 4°C) for 15min and protein concentration was quantified using BCA assay. Protein samples were loaded on a Protean TGX gel (Bio-Rad) and transferred into a PVDF membrane. Membranes were blocked in 5% milk in TBS-Tween 0.1% for 1h at room temperature and primary antibody was incubated overnight at 4°C. Washes were performed in TBS-Tween 0.1% and membranes were incubated with secondary antibodies conjugated to HRP (Amersham) for 1h at room temperature and developed using Western Lightning Plus ECL (Perkin Elmer). Densitometry was performed using Fiji [56].

RNA-sequencing and analysis

Mice were euthanized and perfused with PBS containing 5U/mL heparin. The brain was harvested and coronal slices were cut using an adult mouse matrix (69080-C, Electron Microscopy Sciences). Coronal slices (cut to include bregma −0.88 to −1.855) were prepared from untreated animals (3mm thick) and cuprizone treated animals (2 mm) to normalize total RNA quantity. The corpus callosum was then micro-dissected, flash-frozen in liquid nitrogen, and RNA was extracted using the Isolate II Kit (Bioline). RNA-seq (Illumina) was performed by the Genomic Sciences Lab or the Genome Analysis and Technology Core at the University of Virginia.

Quantified reads mapped to Ensembl gene transcript IDs and imported into the R programming environment with the tximport R package. Gene dispersion values were estimated using DESeq2 (v1.22.1), after which pairwise comparisons were made between cuprizone-fed and untreated mice at each time point (3wk, 5wk, 5.5wk) after cuprizone administration. The resulting differentially expressed genes were selected using a q-value threshold of 0.05. From these lists, any genes that were found to be differentially expressed between *Lrp1*$^{fl/fl}$*Olig1*^{Cre} and *Olig1*^{Cre} mice at 0 weeks after cuprizone administration were removed (Table S2) from the gene lists obtained from pairwise comparisons between genotypes in the subsequent three time points. These gene lists were further subdivided into "up-regulated" and "down-regulated" gene lists using log2 fold change (L2FC) thresholds of ±log2(1.5).

Resulting gene lists from the differential expression analysis were imported into the R package ClusterProfiler (v3.10.1) to perform an over-representation analysis on gene lists against the Gene Ontology Consortium's Biological process (BP) database (v3.7.0). In this implementation, Fischer's exact test was applied to each gene list against a background of all genes in the data set while excluding the genes that were differentially expressed among genotypes before cuprizone administration (0wk). Any Gene Ontology terms with a q-value greater than 0.05 were thrown out as insignificant.

Curated gene lists were made from the lists of differentially expressed genes to represent genes specific for neuroinflammation, myelination and oligodendrocyte identity. The corresponding DESeq2 normalized counts were visualized using the R package pheatmap (v1.0.10) and standardized with z-score normalization across all samples. Upset plots were created using the R package UpSetR (v1.3.3).

Flow cytometry

Flow cytometric analyses were performed as previously described [57]. eBioscience antibodies were used unless otherwise specified: TCRβ (H57–597), CD4 (RM4–5), CD8 (53–6.7), CD19 (eBio1D3), CD45 (30-F11), CD11b (M1/70), CD44 (IM7), CD62L (MEL14), CD11c (N418), Ly6G (1A8), PDGFRα (APA5), O4 (O4; Miltenyi), CD13 (R3–242; BD), CD31 (390; BioLegend), MHC1 (28–8-6; BioLegend), and CD16/CD32 (93). Viability was assessed using a Zombie Aqua Fixable Viability kit (cat. no. 423101, BioLegend) or Ghost Dye Violet 510 (cat. no. 13–0870, Tonbo Biosciences).

Antigen Recall

Single cell suspensions were prepared from inguinal lymph nodes 7 days post-immunization as previously described [57]. Cells were treated with various concentrations of $MOG_{35–55}$ peptide for 48–72h and the concentration of secreted IFN-γ and IL-17A was determined using a Luminex multiplex immunoassay.

Primary OPC cultures

Primary OPC cultures were prepared from P4–8 mouse pups as previously described with minor modifications [18]. In short, cortices were dissected and the meninges was removed before being digested in 4–5mL Accutase (A1110501, Thermo Fisher) for 45min at 37°C in

5% CO_2 and triturating every 15min. Cell suspensions were then filtered through a 40μm strainer, spun down, resuspended in panning buffer, and sequentially incubated in two BSL-1 plates, and finally a rat anti-PDGFRα (APA5) coated plate to select for OPCs. Cells were cultured and expanded for 6 days in poly-L-lysine coated tissue culture plates in OPC proliferation media (DMEM, Pen/Strep, B27, N2, CNTF, NT-3, PDGF-AA, forskolin), and then replated in OPC differentiation media (DMEM, B27, N2, CNTF, T3, forskolin) for 2–3 days to generate oligodendrocytes for gene expression analysis.

The following assay was performed by Renovo Neural (Cleveland, OH). In brief, OPCs from *Plp*-EGFP mice were plated at a density of ~7,000 cells per well in a 96-well plate. Cells were treated with RAP, 0.1% DMSO, and T3 (six wells per condition) in OPC differentiation media for 5 days, with one media change at 48h. Cells were then fixed with 4% PFA, stained with Hoechst, and 20 images per well were captured using a Cellomics VTI scanner. Total and pyknotic nuclei, as well as $EGFP^+$ cells were quantified.

Antigen Cross-Presentation Assay

Assay was performed as described with minor modifications[40]. Cultured OPCs were plated in a 96-well plate at 20,000 cells per well. The next day, OPCs were treated with 10ng/mL IFNγ for 12h. OPCs were then pre-treated with 300nM GST-RAP or GST (vehicle) for 1h in IFNγ-containing OPC media. Next, OPCs were incubated with 500μg/mL of OVA (77120, Thermo Fisher) in IFNγ-containing OPC media in the presence of GST-RAP or GST for 8h. During the 8h OVA incubation, OT-I CD8 T cells were isolated (19853, Stem Cell Technologies) from spleen and lymph nodes and labeled with Cell Proliferation Dye e450 (65–0842-85, eBioscience). OPCs were then washed with PBS and 160,000 OT-I CD8 T cells were added in a 50/50 mix of RPMI complete and OPC media. OT-I CD8 T cell proliferation was examined using flow cytometry after 48h of coculture.

RT-qPCR

RNA was extracted using the Isolate II Kit (Bioline). cDNA was prepared using iScript cDNA Synthesis Kit (Bio-Rad) or SensiFAST cDNA Synthesis Kit (Bioline). RT-qPCR was performed using NO-ROX SensiFAST Probe or SYBR Mix (Bioline). Taqman probes (Thermo Fisher) were used for *Mbp*, *Cnp*, *Lrp1*, and *Gapdh*. Primers were used for *Mrf* (Forward: CGGCGTCTCGACAGCCTCAA, Reverse: GACACGGCAAGAGAGCCGTCA). Samples were run and analyzed on a PikoReal PCR system (Thermo Fisher).

Statistical Analyses

All statistical analyses were performed in Prism 8 (GraphPad software). The results of the statistical tests are presented within the results section. For all analyses, significance was set at $p<0.05$. Repeats for each experiment, are indicated in the figure legend corresponding to the respective panel.

Supplementary Material

Refer to Web version on PubMed Central for supplementary material.

Acknowledgements

We thank Dr. Sanja Arandjelovic and Courtney Rivet-Noor (University of Virginia) for critical reading of the manuscript. We thank Dr. Ioana A. Marin (Stanford) for insightful scientific discussions. Dr. Timothy Bullock (University of Virginia) generously provided OT-I mice for this study. The authors are supported by grants from the NINDS R01 NS083542 and R21 NS111204, the National Multiple Sclerosis Society PP1978 and the Owens family foundation. A.F.C. is supported by T32 GM008328. D.A.R. is supported by T32 GM007055. S.M.S. is supported by T32 GM007267 and F31 NS103327.

References

1. Ajami B, Bennett JL, Krieger C, McNagny KM, Rossi FM (2011) Infiltrating monocytes trigger EAE progression, but do not contribute to the resident microglia pool. Nat Neurosci 14: 1142–1149 Doi 10.1038/nn.2887 [PubMed: 21804537]
2. Arnett HA, Fancy SP, Alberta JA, Zhao C, Plant SR, Kaing S, Raine CS, Rowitch DH, Franklin RJ, Stiles CD (2004) bHLH transcription factor Olig1 is required to repair demyelinated lesions in the CNS. Science 306: 2111–2115 Doi 10.1126/science.1103709 [PubMed: 15604411]
3. Auderset L, Cullen CL, Young KM (2016) Low Density Lipoprotein-Receptor Related Protein 1 Is Differentially Expressed by Neuronal and Glial Populations in the Developing and Mature Mouse Central Nervous System. PLoS One 11: e0155878 Doi 10.1371/journal.pone.0155878 [PubMed: 27280679]
4. Back SA, Tuohy TM, Chen H, Wallingford N, Craig A, Struve J, Luo NL, Banine F, Liu Y, Chang Aet al. (2005) Hyaluronan accumulates in demyelinated lesions and inhibits oligodendrocyte progenitor maturation. Nat Med 11: 966–972 Doi 10.1038/nm1279 [PubMed: 16086023]
5. Basu S, Binder RJ, Ramalingam T, Srivastava PK (2001) CD91 is a common receptor for heat shock proteins gp96, hsp90, hsp70, and calreticulin. Immunity 14: 303–313 [PubMed: 11290339]
6. Behjati S, Frank MH (2009) The effects of tamoxifen on immunity. Curr Med Chem 16: 3076–3080 [PubMed: 19689284]
7. Binder RJ, Han DK, Srivastava PK (2000) CD91: a receptor for heat shock protein gp96. Nature immunology 1: 151–155 Doi 10.1038/77835 [PubMed: 11248808]
8. Binder RJ, Srivastava PK (2004) Essential role of CD91 in re-presentation of gp96-chaperoned peptides. Proc Natl Acad Sci U S A 101: 6128–6133 Doi 10.1073/pnas.0308180101010308180101 [pii] [PubMed: 15073331]
9. Brifault C, Gilder AS, Laudati E, Banki M, Gonias SL (2017) Shedding of membrane-associated LDL receptor-related protein-1 from microglia amplifies and sustains neuroinflammation. The Journal of biological chemistry 292: 18699–18712 Doi 10.1074/jbc.M117.798413 [PubMed: 28972143]
10. Butovsky O, Landa G, Kunis G, Ziv Y, Avidan H, Greenberg N, Schwartz A, Smirnov I, Pollack A, Jung Set al (2006) Induction and blockage of oligodendrogenesis by differently activated microglia in an animal model of multiple sclerosis. J Clin Invest 116: 905–915 Doi 10.1172/JCI26836 [PubMed: 16557302]
11. Butti E, Bacigaluppi M, Chaabane L, Ruffini F, Brambilla E, Berera G, Montonati C, Quattrini A, Martino G (2019) Neural Stem Cells of the Subventricular Zone Contribute to Neuroprotection of the Corpus Callosum after Cuprizone-Induced Demyelination. J Neurosci 39: 5481–5492 Doi 10.1523/JNEUROSCI.0227-18.2019 [PubMed: 31138656]
12. Cantuti-Castelvetri L, Fitzner D, Bosch-Queralt M, Weil MT, Su M, Sen P, Ruhwedel T, Mitkovski M, Trendelenburg G, Lutjohann Det al. (2018) Defective cholesterol clearance limits remyelination in the aged central nervous system. Science 359: 684–688 Doi 10.1126/science.aan4183 [PubMed: 29301957]
13. Chang A, Tourtellotte WW, Rudick R, Trapp BD (2002) Premyelinating oligodendrocytes in chronic lesions of multiple sclerosis. N Engl J Med 346: 165–173 Doi 10.1056/NEJMoa010994 [PubMed: 11796850]
14. Chew LJ, King WC, Kennedy A, Gallo V (2005) Interferon-gamma inhibits cell cycle exit in differentiating oligodendrocyte progenitor cells. Glia 52: 127–143 Doi 10.1002/glia.20232 [PubMed: 15920731]

15. Chuang TY, Guo Y, Seki SM, Rosen AM, Johanson DM, Mandell JW, Lucchinetti CF, Gaultier A (2016) LRP1 expression in microglia is protective during CNS autoimmunity. Acta neuropathologica communications 4: 68 Doi 10.1186/s40478-016-0343-2 [PubMed: 27400748]

16. Dai J, Bercury KK, Ahrendsen JT, Macklin WB (2015) Olig1 function is required for oligodendrocyte differentiation in the mouse brain. J Neurosci 35: 4386–4402 Doi 10.1523/JNEUROSCI.4962-14.2015 [PubMed: 25762682]

17. Denker SP, Ji S, Dingman A, Lee SY, Derugin N, Wendland MF, Vexler ZS (2007) Macrophages are comprised of resident brain microglia not infiltrating peripheral monocytes acutely after neonatal stroke. J Neurochem 100: 893–904 Doi 10.1111/j.1471-4159.2006.04162.x [PubMed: 17212701]

18. Emery B, Dugas JC (2013) Purification of oligodendrocyte lineage cells from mouse cortices by immunopanning. Cold Spring Harb Protoc 2013: 854–868 Doi 10.1101/pdb.prot073973 [PubMed: 24003195]

19. Falcao AM, van Bruggen D, Marques S, Meijer M, Jakel S, Agirre E, Samudyata, Floriddia EM, Vanichkina DP, Ffrench-Constant Cet al. (2018) Disease-specific oligodendrocyte lineage cells arise in multiple sclerosis. Nat Med 24: 1837–1844 Doi 10.1038/s41591-018-0236-y [PubMed: 30420755]

20. Fernandez-Castaneda A, Arandjelovic S, Stiles TL, Schlobach RK, Mowen KA, Gonias SL, Gaultier A (2013) Identification of the low density lipoprotein (LDL) receptor-related protein-1 interactome in central nervous system myelin suggests a role in the clearance of necrotic cell debris. J Biol Chem 288: 4538–4548 Doi 10.1074/jbc.M112.384693 [PubMed: 23264627]

21. Fernandez-Castaneda A, Gaultier A (2016) Adult oligodendrocyte progenitor cells - Multifaceted regulators of the CNS in health and disease. Brain Behav Immun 57: 1–7 Doi 10.1016/j.bbi.2016.01.005 [PubMed: 26796621]

22. Ford ML, Evavold BD (2005) Specificity, magnitude, and kinetics of MOG-specific CD8+ T cell responses during experimental autoimmune encephalomyelitis. European journal of immunology 35: 76–85 Doi 10.1002/eji.200425660 [PubMed: 15593305]

23. Franklin RJ (2002) Why does remyelination fail in multiple sclerosis? Nat Rev Neurosci 3: 705–714 Doi 10.1038/nrn917 [PubMed: 12209119]

24. Gaultier A, Arandjelovic S, Niessen S, Overton CD, Linton MF, Fazio S, Campana WM, Cravatt BF 3rd, Gonias SL (2008) Regulation of tumor necrosis factor receptor-1 and the IKK-NF-kappaB pathway by LDL receptor-related protein explains the antiinflammatory activity of this receptor. Blood 111: 5316–5325 Doi 10.1182/blood-2007-12-127613 [PubMed: 18369152]

25. Gaultier A, Hollister M, Reynolds I, Hsieh EH, Gonias SL (2010) LRP1 regulates remodeling of the extracellular matrix by fibroblasts. Matrix Biol 29: 22–30 Doi 10.1016/j.matbio.2009.08.003 [PubMed: 19699300]

26. Gaultier A, Wu X, Le Moan N, Takimoto S, Mukandala G, Akassoglou K, Campana WM, Gonias SL (2009) Low-density lipoprotein receptor-related protein 1 is an essential receptor for myelin phagocytosis. J Cell Sci 122: 1155–1162 Doi 10.1242/jcs.040717 [PubMed: 19299462]

27. Goldberg J, Daniel M, van Heuvel Y, Victor M, Beyer C, Clarner T, Kipp M (2013) Short-term cuprizone feeding induces selective amino acid deprivation with concomitant activation of an integrated stress response in oligodendrocytes. Cellular and molecular neurobiology 33: 1087–1098 Doi 10.1007/s10571-013-9975-y [PubMed: 23979168]

28. Goldmann T, Wieghofer P, Muller PF, Wolf Y, Varol D, Yona S, Brendecke SM, Kierdorf K, Staszewski O, Datta Met al. (2013) A new type of microglia gene targeting shows TAK1 to be pivotal in CNS autoimmune inflammation. Nat Neurosci 16: 1618–1626 Doi 10.1038/nn.3531 [PubMed: 24077561]

29. Gong S, Zheng C, Doughty ML, Losos K, Didkovsky N, Schambra UB, Nowak NJ, Joyner A, Leblanc G, Hatten MEet al. (2003) A gene expression atlas of the central nervous system based on bacterial artificial chromosomes. Nature 425: 917–925 Doi 10.1038/nature02033 [PubMed: 14586460]

30. Gonias SL, Campana WM (2014) LDL receptor-related protein-1: a regulator of inflammation in atherosclerosis, cancer, and injury to the nervous system. Am J Pathol 184: 18–27 Doi 10.1016/j.ajpath.2013.08.029 [PubMed: 24128688]

31. Gonzalez GA, Hofer MP, Syed YA, Amaral AI, Rundle J, Rahman S, Zhao C, Kotter MR (2016) Tamoxifen accelerates the repair of demyelinated lesions in the central nervous system. Scientific reports 6: 31599 Doi 10.1038/srep31599 [PubMed: 27554391]
32. Hart JP, Gunn MD, Pizzo SV (2004) A CD91-positive subset of CD11c+ blood dendritic cells: characterization of the APC that functions to enhance adaptive immune responses against CD91-targeted antigens. J Immunol 172: 70–78 [PubMed: 14688311]
33. Herz J, Goldstein JL, Strickland DK, Ho YK, Brown MS (1991) 39-kDa protein modulates binding of ligands to low density lipoprotein receptor-related protein/alpha 2-macroglobulin receptor. J Biol Chem 266: 21232–21238 [PubMed: 1718973]
34. Hughes EG, Kang SH, Fukaya M, Bergles DE (2013) Oligodendrocyte progenitors balance growth with self-repulsion to achieve homeostasis in the adult brain. Nat Neurosci 16: 668–676 Doi 10.1038/nn.3390 [PubMed: 23624515]
35. Huseby ES, Liggitt D, Brabb T, Schnabel B, Ohlen C, Goverman J (2001) A pathogenic role for myelin-specific CD8(+) T cells in a model for multiple sclerosis. J Exp Med 194: 669–676 Doi 10.1084/jem.194.5.669 [PubMed: 11535634]
36. Irvine KA, Blakemore WF (2008) Remyelination protects axons from demyelination-associated axon degeneration. Brain 131: 1464–1477 Doi 10.1093/brain/awn080 [PubMed: 18490361]
37. Kang Z, Wang C, Zepp J, Wu L, Sun K, Zhao J, Chandrasekharan U, DiCorleto PE, Trapp BD, Ransohoff RMet al. (2013) Act1 mediates IL-17-induced EAE pathogenesis selectively in NG2+ glial cells. Nat Neurosci 16: 1401–1408 Doi 10.1038/nn.3505 [PubMed: 23995070]
38. Kipp M, Clarner T, Dang J, Copray S, Beyer C (2009) The cuprizone animal model: new insights into an old story. Acta neuropathologica 118: 723–736 Doi 10.1007/s00401-009-0591-3 [PubMed: 19763593]
39. Kirby L, Jin J, Gonzalez-Cardona J, Smith M, Martin K, Wang J, Strasburger H, Herbst L, Alexis M, Karnell Jet al. (2018) Oligodendrocyte Precursor Cells Are Co-Opted by the Immune System to Cross-Present Antigen and Mediate Cytotoxicity. bioRxiv: 461434 Doi 10.1101/461434
40. Kirby LA, Jin J, Gonzalez-Cardona J, Smyith M, Martin K, Wang J, Strasburger H, Herbst L, Alexis M, Karneli Jet al. (2018) Oligodendrocyte Precursor Cells Are Co-Opted by the Immune System to Cross-Present Antigen and Mediate Cytotoxicity. bioRxiv 461434: Doi 10.1101/461434
41. Kotter MR, Li WW, Zhao C, Franklin RJ (2006) Myelin impairs CNS remyelination by inhibiting oligodendrocyte precursor cell differentiation. J Neurosci 26: 328–332 Doi 10.1523/JNEUROSCI.2615-05.2006 [PubMed: 16399703]
42. Kuhlmann T, Miron V, Cui Q, Wegner C, Antel J, Bruck W (2008) Differentiation block of oligodendroglial progenitor cells as a cause for remyelination failure in chronic multiple sclerosis. Brain 131: 1749–1758 Doi 10.1093/brain/awn096 [PubMed: 18515322]
43. Lau LW, Keough MB, Haylock-Jacobs S, Cua R, Doring A, Sloka S, Stirling DP, Rivest S, Yong VW (2012) Chondroitin sulfate proteoglycans in demyelinated lesions impair remyelination. Ann Neurol 72: 419–432 Doi 10.1002/ana.23599 [PubMed: 23034914]
44. Lillis AP, Van Duyn LB, Murphy-Ullrich JE, Strickland DK (2008) LDL Receptor-Related Protein 1: Unique Tissue-Specific Functions Revealed by Selective Gene Knockout Studies. Physiol Rev 88: 887–918 [PubMed: 18626063]
45. Lin JP, Mironova YA, Shrager P, Giger RJ (2017) LRP1 regulates peroxisome biogenesis and cholesterol homeostasis in oligodendrocytes and is required for proper CNS myelin development and repair. eLife 6: Doi 10.7554/eLife.30498
46. Lin W, Kemper A, Dupree JL, Harding HP, Ron D, Popko B (2006) Interferon-gamma inhibits central nervous system remyelination through a process modulated by endoplasmic reticulum stress. Brain 129: 1306–1318 Doi 10.1093/brain/awl044 [PubMed: 16504972]
47. Lu QR, Sun T, Zhu Z, Ma N, Garcia M, Stiles CD, Rowitch DH (2002) Common developmental requirement for Olig function indicates a motor neuron/oligodendrocyte connection. Cell 109: 75–86 [PubMed: 11955448]
48. Mantuano E, Brifault C, Lam MS, Azmoon P, Gilder AS, Gonias SL (2016) LDL receptor-related protein-1 regulates NFkappaB and microRNA-155 in macrophages to control the inflammatory response. Proc Natl Acad Sci U S A 113: 1369–1374 Doi 10.1073/pnas.1515480113 [PubMed: 26787872]

49. Marcus J, Honigbaum S, Shroff S, Honke K, Rosenbluth J, Dupree JL (2006) Sulfatide is essential for the maintenance of CNS myelin and axon structure. Glia 53: 372–381 Doi 10.1002/glia.20292 [PubMed: 16288467]
50. May P, Rohlmann A, Bock HH, Zurhove K, Marth JD, Schomburg ED, Noebels JL, Beffert U, Sweatt JD, Weeber EJet al. (2004) Neuronal LRP1 functionally associates with postsynaptic proteins and is required for normal motor function in mice. Mol Cell Biol 24: 8872–8883 [PubMed: 15456862]
51. Na SY, Cao Y, Toben C, Nitschke L, Stadelmann C, Gold R, Schimpl A, Hunig T (2008) Naive CD8 T-cells initiate spontaneous autoimmunity to a sequestered model antigen of the central nervous system. Brain 131: 2353–2365 Doi 10.1093/brain/awn148 [PubMed: 18669487]
52. Na SY, Eujen H, Gobel K, Meuth SG, Martens K, Wiendl H, Hunig T (2009) Antigen-specific blockade of lethal CD8 T-cell mediated autoimmunity in a mouse model of multiple sclerosis. J Immunol 182: 6569–6575 Doi 10.4049/jimmunol.0804200 [PubMed: 19414812]
53. Raasch J, Zeller N, van Loo G, Merkler D, Mildner A, Erny D, Knobeloch KP, Bethea JR, Waisman A, Knust Met al. (2011) IkappaB kinase 2 determines oligodendrocyte loss by non-cell-autonomous activation of NF-kappaB in the central nervous system. Brain 134: 1184–1198 Doi 10.1093/brain/awq359 [PubMed: 21310728]
54. Ransohoff RM (2012) Animal models of multiple sclerosis: the good, the bad and the bottom line. Nat Neurosci 15: 1074–1077 Doi 10.1038/nn.3168 [PubMed: 22837037]
55. Sachs HH, Bercury KK, Popescu DC, Narayanan SP, Macklin WB (2014) A new model of cuprizone-mediated demyelination/remyelination. ASN neuro 6: Doi 10.1177/1759091414551955
56. Schindelin J, Arganda-Carreras I, Frise E, Kaynig V, Longair M, Pietzsch T, Preibisch S, Rueden C, Saalfeld S, Schmid Bet al. (2012) Fiji: an open-source platform for biological-image analysis. Nature methods 9: 676–682 Doi 10.1038/nmeth.2019 [PubMed: 22743772]
57. Seki SM, Stevenson M, Rosen AM, Arandjelovic S, Gemta L, Bullock TNJ, Gaultier A (2017) Lineage-Specific Metabolic Properties and Vulnerabilities of T Cells in the Demyelinating Central Nervous System. J Immunol 198: 4607–4617 Doi 10.4049/jimmunol.1600825 [PubMed: 28507026]
58. Skripuletz T, Gudi V, Hackstette D, Stangel M (2011) De- and remyelination in the CNS white and grey matter induced by cuprizone: the old, the new, and the unexpected. Histol Histopathol 26: 1585–1597 [PubMed: 21972097]
59. Song H, Li Y, Lee J, Schwartz AL, Bu G (2009) Low-density lipoprotein receptor-related protein 1 promotes cancer cell migration and invasion by inducing the expression of matrix metalloproteinases 2 and 9. Cancer Res 69: 879–886 Doi 10.1158/0008-5472.CAN-08-3379 [PubMed: 19176371]
60. Subramanian M, Hayes CD, Thome JJ, Thorp E, Matsushima GK, Herz J, Farber DL, Liu K, Lakshmana M, Tabas I (2014) An AXL/LRP-1/RANBP9 complex mediates DC efferocytosis and antigen cross-presentation in vivo. J Clin Invest 124: 1296–1308 Doi 10.1172/JCI72051 [PubMed: 24509082]
61. Yang L, Liu CC, Zheng H, Kanekiyo T, Atagi Y, Jia L, Wang D, N'Songo A, Can D, Xu Het al. (2016) LRP1 modulates the microglial immune response via regulation of JNK and NF-kappaB signaling pathways. J Neuroinflammation 13: 304 Doi 10.1186/s12974-016-0772-7 [PubMed: 27931217]
62. Zhang N, Bevan MJ (2011) CD8(+) T cells: foot soldiers of the immune system. Immunity 35: 161–168 Doi 10.1016/j.immuni.2011.07.010 [PubMed: 21867926]
63. Zhang Y, Chen K, Sloan SA, Bennett ML, Scholze AR, O'Keeffe S, Phatnani HP, Guarnieri P, Caneda C, Ruderisch Net al. (2014) An RNA-sequencing transcriptome and splicing database of glia, neurons, and vascular cells of the cerebral cortex. J Neurosci 34: 11929–11947 Doi 10.1523/JNEUROSCI.1860-14.2014 [PubMed: 25186741]

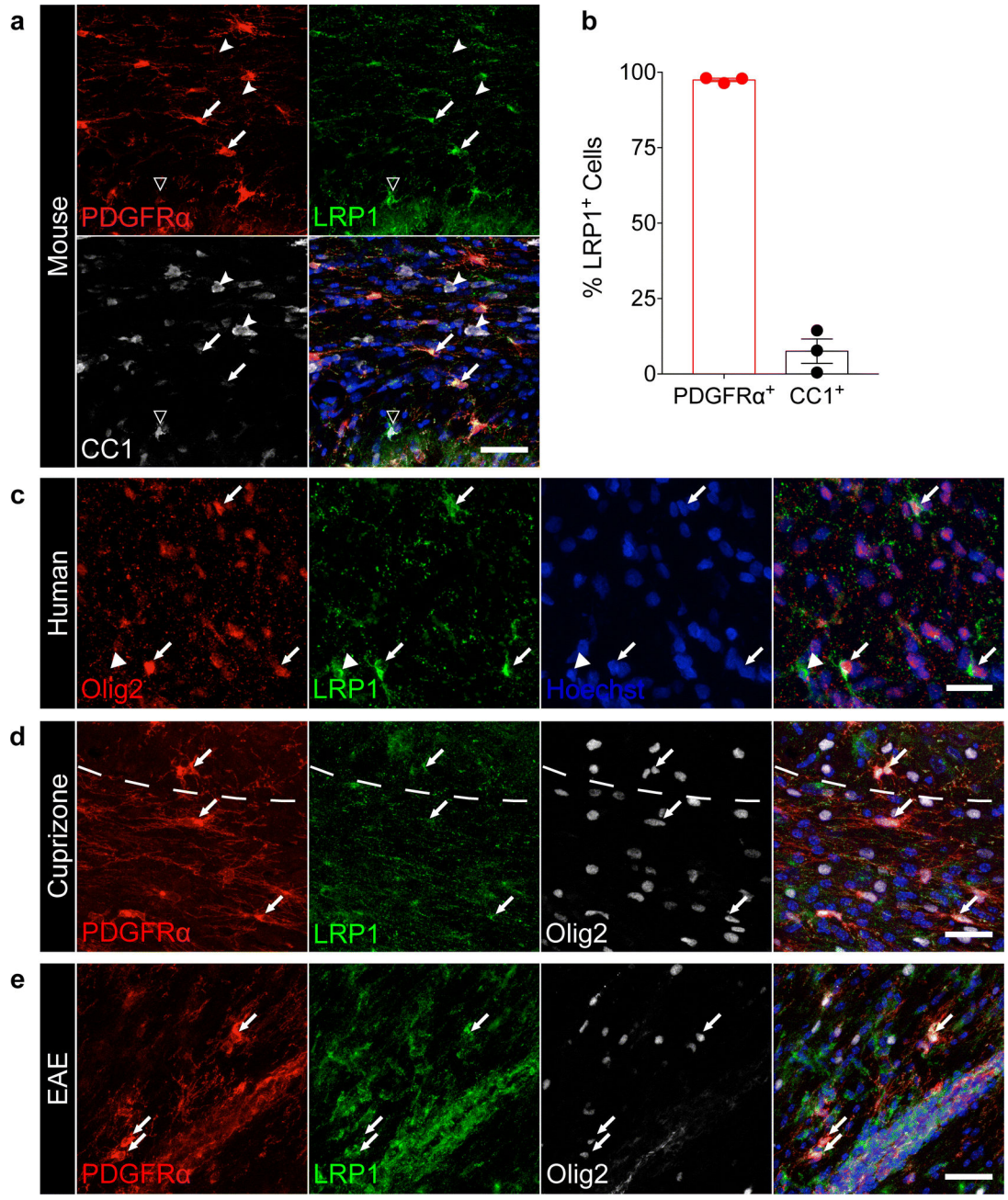

Fig. 1. LRP1 is dynamically expressed in oligodendroglia in the homeostatic and pathological CNS

(**a**) Staining in the adult mouse *corpus callosum* for PDGFRα, LRP1, and CC1 (arrows = PDGFRα$^+$ LRP1$^+$ cells; dented arrowheads = CC1$^+$ LRP1$^-$ cells; hollow arrowhead = CC1$^+$ LRP1$^+$ cell). Scale bar 40μm. (**b**) Quantification of PDGFRα$^+$ and CC1$^+$ cells expressing LRP1 in the adult mouse *corpus callosum* (n=3 mice; error bars represent +/− SEM). (**c**) Human white matter stained for Olig2 and LRP1 (arrows = Olig2$^+$ LRP1$^+$ cells; arrowheads = Olig2$^-$ LRP1$^+$ cells). Scale bar 20μm. (**d**) Staining for PDGFRα, LRP1, and Olig2 in the mouse *corpus callosum* after cuprizone-induced demyelination (arrows = PDGFRα$^+$ LRP1$^+$ Olig2$^+$ cells). Dashed line demarcates the border between the cortex and corpus callosum.

Scale bar 30μm. (**e**) EAE spinal cord stained for PDGFRα, LRP1, and Olig2 (arrows = $PDGFR\alpha^+$ $LRP1^+$ $Olig2^+$ cells). Scale bar 40μm.

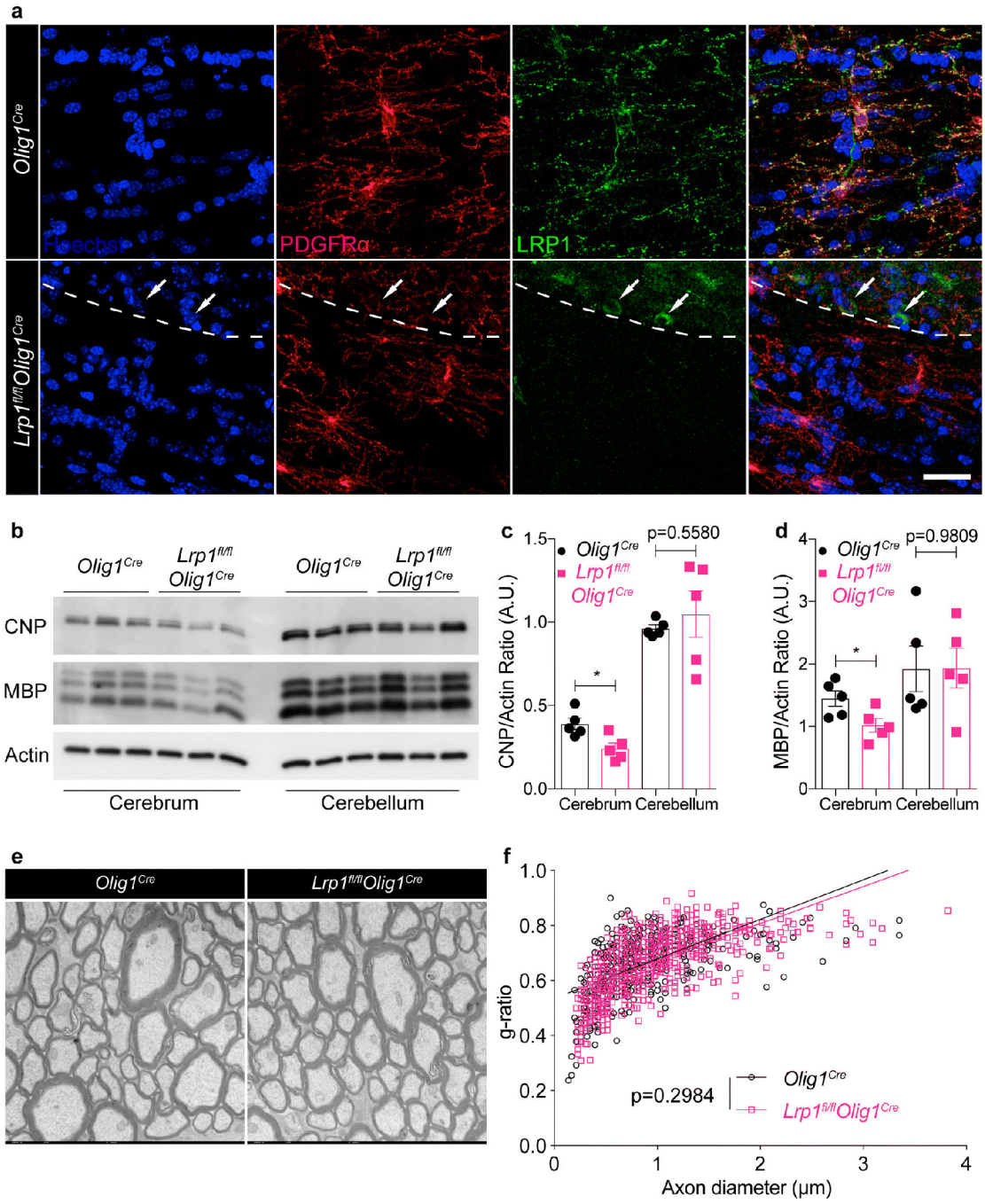

Fig. 2. Deletion of LRP1 in OPCs is not associated with severe myelin defects

(**a**) Staining for PDGFRα and LRP1 in the *corpus callosum* in *Olig1*^{cre} and *Lrp1*$^{fl/fl}$*Olig1*^{cre} mice (arrows = LRP1^{+} PDGFRα^{-} cells). Dashed line demarcates the border between the cortex and *corpus callosum*. Scale bar 25μm. (**b**) Representative immunoblot and (**c**,**d**) densitometry analysis for CNP, MBP, and actin from cerebrum and cerebellum (unpaired t-test, MBP *p=0.0329, CNP *p=0.0150; n=5 mice per genotype, 2 independent experiments combined; error bars represent +/− SEM). (**e**) Representative TEM images and (**f**) calculated

g-ratio of optic nerves (6,000x magnification; n=4 mice per genotype, 10 fields per mouse; linear regression analysis with slopes comparison).

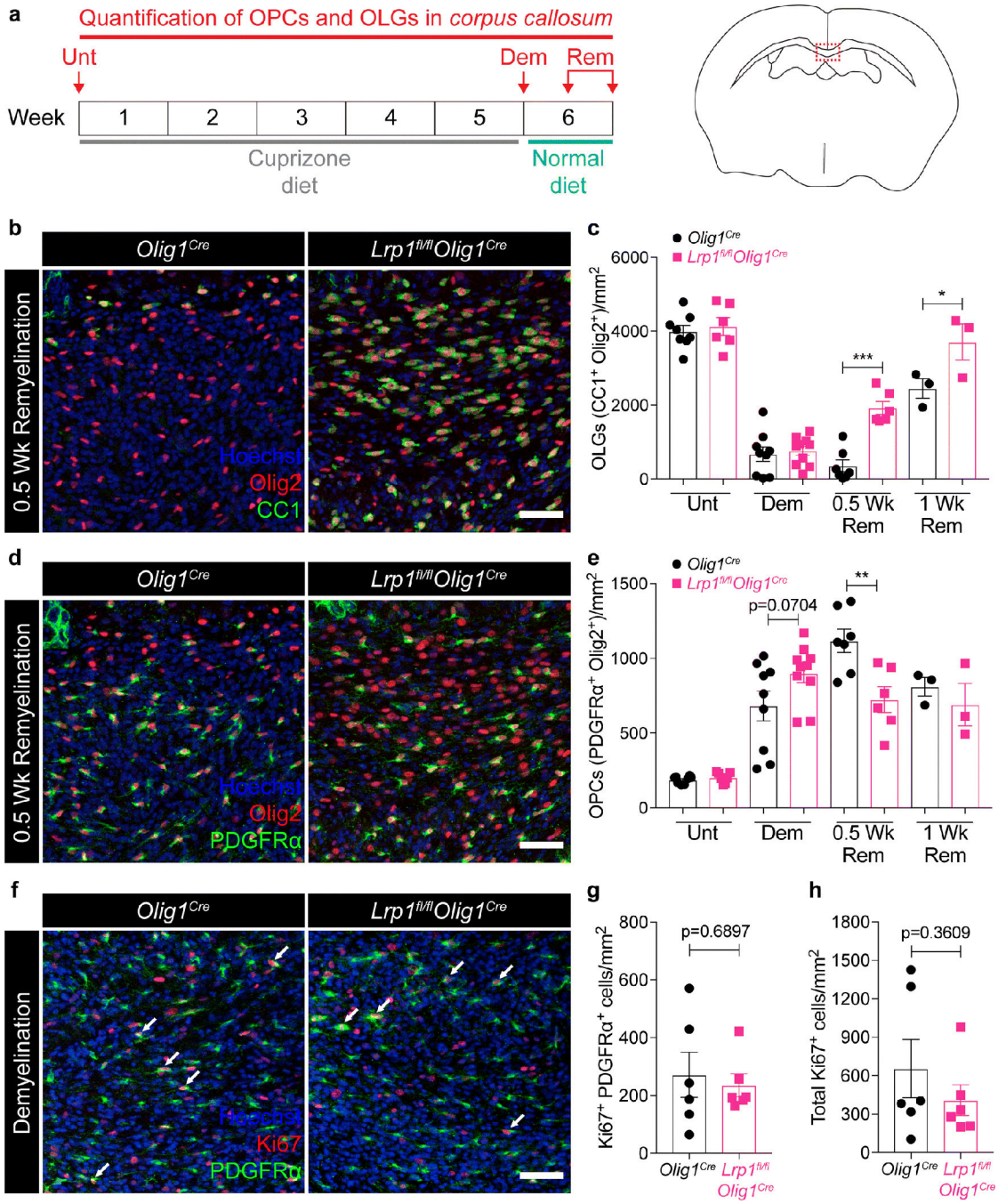

Fig. 3. Mice lacking LRP1 in OPCs display enhanced oligodendrogenesis after cuprizone-induced demyelination

(**a**) Schematic illustrating the cuprizone diet timeline and the timepoints at which the *corpus callosum* was imaged in *Olig1*^{cre} and *Lrp1*$^{fl/fl}$*Olig1*^{cre} mice. (**b**) Representative images and (**c**) quantification of oligodendrocytes (CC1^{+} Olig2^{+} cells) in the remyelinating *corpus callosum* (Two-way ANOVA with Sidak's multiple comparisons test, *p=0.0153, ***p<0.0001; 3 independent experiments combined). (**d**) Representative images and (**e**) quantification of OPCs (PDGFRα^{+} Olig2^{+} cells) in the remyelinating *corpus callosum*

(Two-way ANOVA with Sidak's multiple comparisons test, **p=0.0027; 3 independent experiments combined). (**f**) Ki67 and PDGFRα staining in the *corpus callosum* at the peak of demyelination (arrows = $Ki67^+$ $PDGFR\alpha^+$ cells). (**g**) Quantification of $Ki67^+$ $PDGFR\alpha^+$ cells and (**h**) total $Ki67^+$ cells in the *corpus callosum* at the peak of demyelination (unpaired t-test; 2 independent experiments combined). Each data point represents an individual mouse. All error bars represent +/− SEM. All scale bars 50μm.

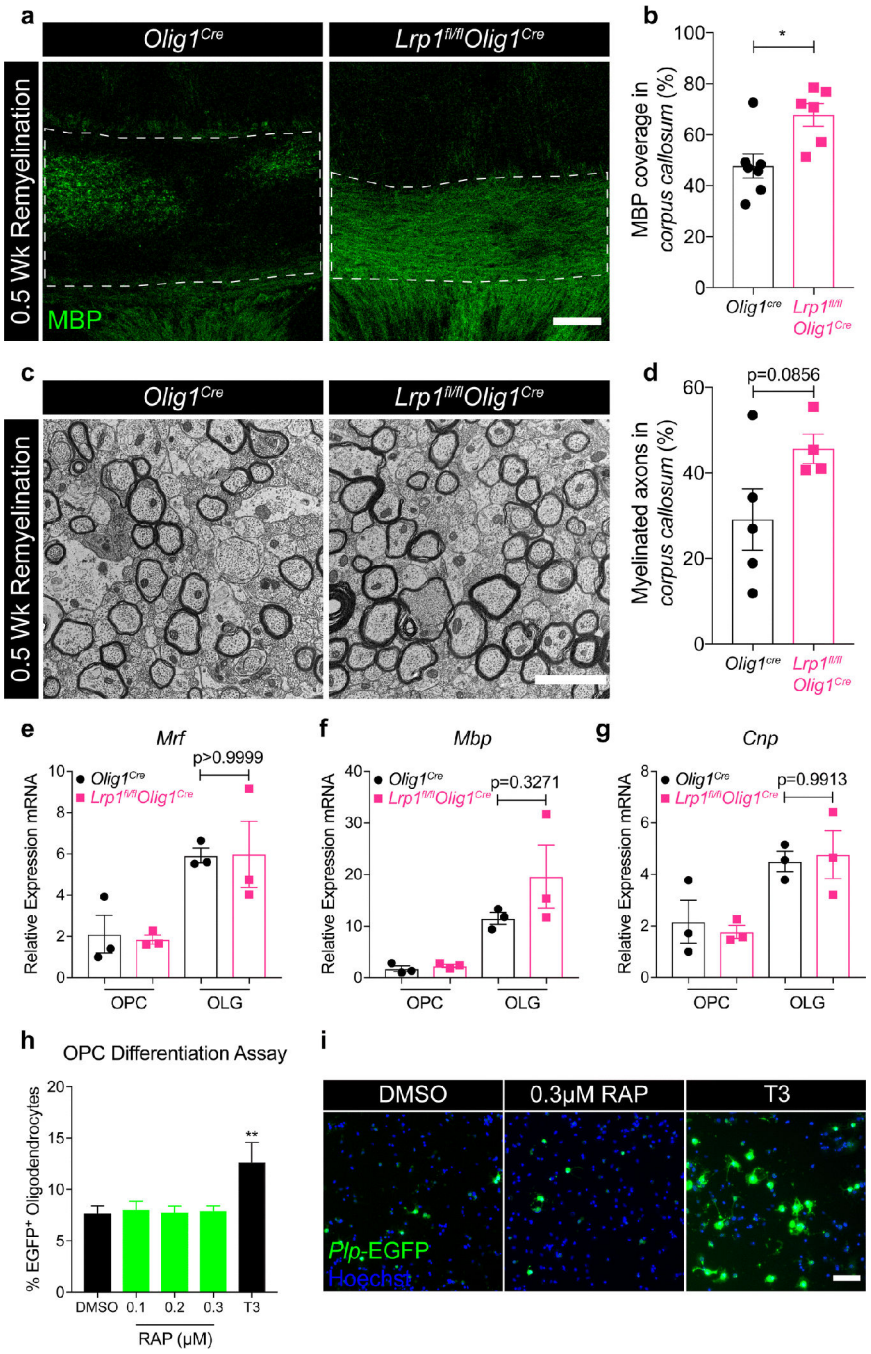

Fig. 4. Enhanced remyelination in mice lacking oligodendroglial LRP1 is not cell-autonomous

(**a**) Representative images and (**b**) quantification of MBP expression in the remyelinating *corpus callosum* of *Olig1*^{cre} and *Lrp1*$^{fl/fl}$*Olig1*^{cre} mice after 0.5 Wk Rem (unpaired t-test; 2 independent experiments combined; scale bar 100μm). (**c**) Representative TEM images and (**d**) quantification of axons in the remyelinating *corpus callosum* after 0.5 Wk Rem (unpaired t-test; n=4–5 mice per genotype; scale bar 2μm). (**e-g**) qPCR for *Mrf*, *Mbp*, and *Cnp* from primary OPCs cultured in proliferation (OPC) or differentiation (OLG) media (unpaired t-test; n=3 mice per genotype). (**h**) Quantification and (**i**) representative images of

Plp-EGFP OPCs treated with DMSO, T3, or increasing concentrations of the specific LRP1 inhibitor, RAP (One-way ANOVA with Dunnett's multiple comparisons test, DMSO vs T3 **p=0.0072; conditions plated in sextuplicate; error bars represent +/− SEM; scale bar 150μm).

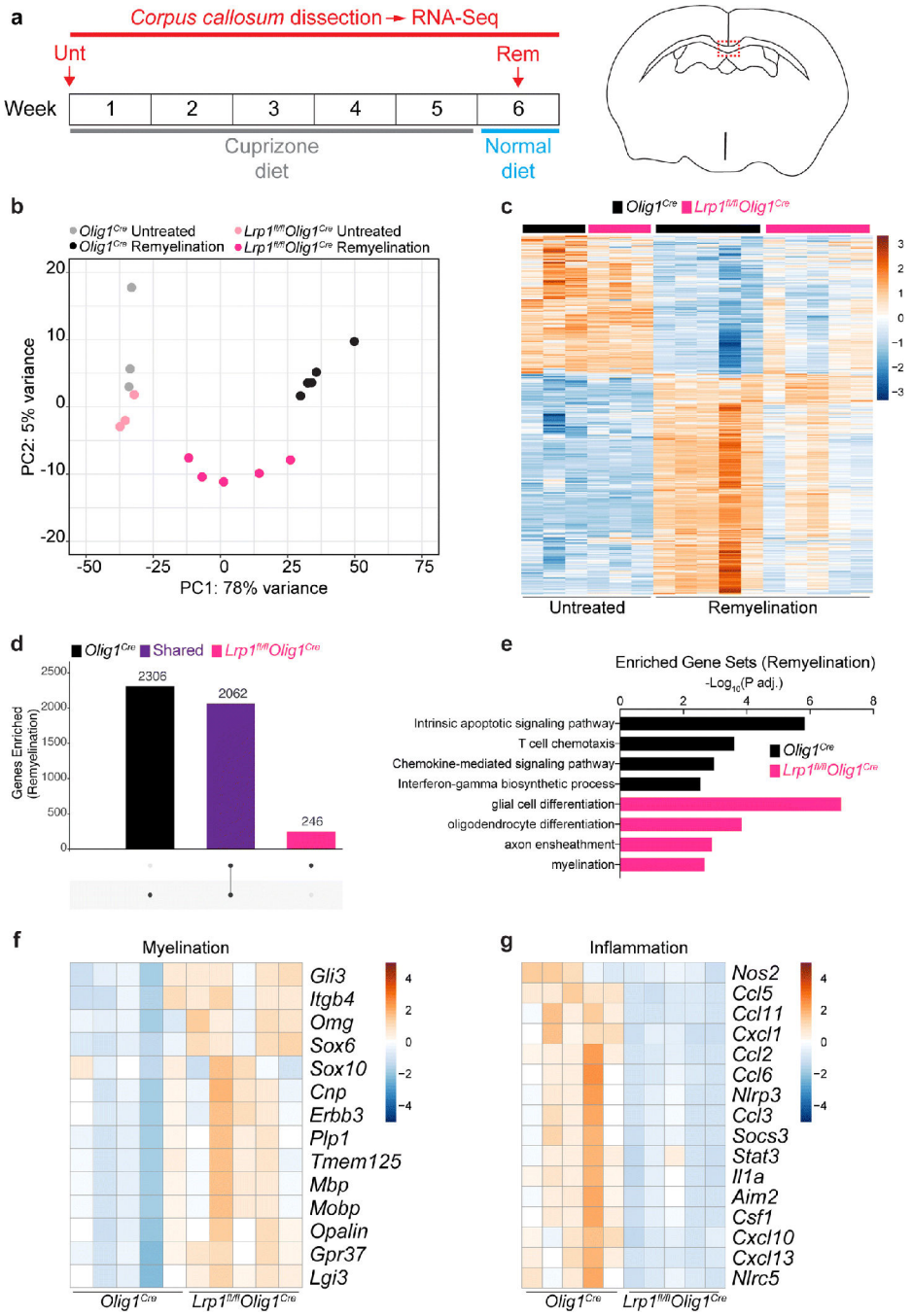

Fig. 5. Oligodendroglial LRP1 modulates the inflammatory landscape and enhances myelin repair

(**a**) Schematic illustrating the cuprizone diet timeline and timepoints at which the *corpus callosum* was dissected and analyzed by RNA-seq. (**b**) Principal component analysis (PCA) plot and (**c**) heat map of the transcriptomes of $Olig1^{cre}$ and $Lrp1^{fl/fl}Olig1^{cre}$ mice. (**d**) UpSet plot showing the number of significantly upregulated genes (compared to untreated mice) that are unique (single dots) or shared (connected dots) in mice undergoing remyelination. (**e**) Gene ontology (GO) terms illustrating unique biological processes upregulated in the

remyelinating *corpus callosum* of *Olig1*^{cre} and *Lrp1*$^{fl/fl}$*Olig1*^{cre} mice. (**f**) Heat maps for myelination- and (**g**) inflammation-related genes in the remyelinating *corpus callosum*. Heat maps have a normalized count scale with z-score normalization.

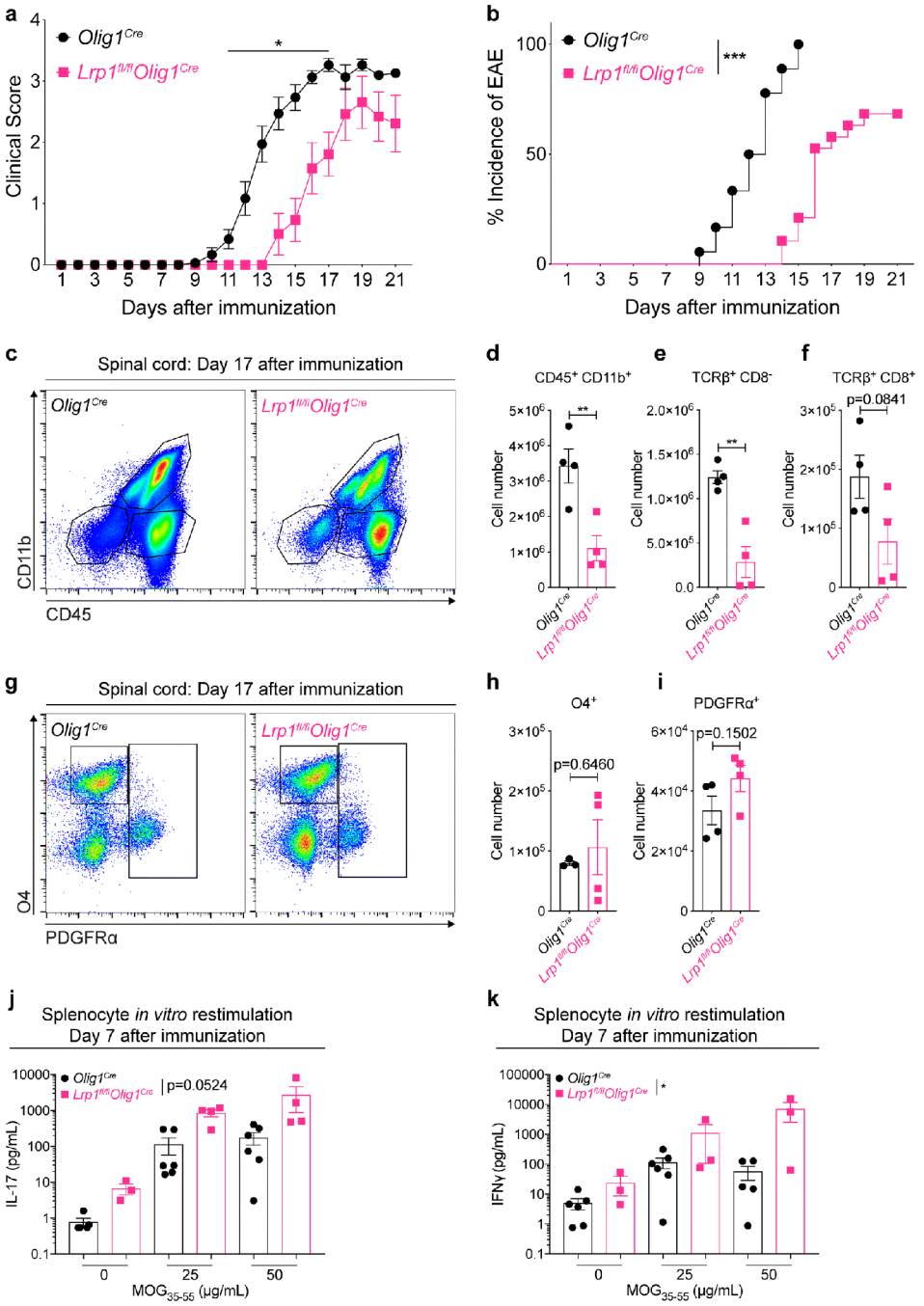

Fig. 6. Deletion of LRP1 in OPCs is protective in experimental autoimmune encephalomyelitis

(**a**) EAE clinical scores and (**b**) incidence of disease in *Olig1*^{cre} and *Lrp1*$^{fl/fl}$*Olig1*^{cre} female mice (EAE scores: Mann-Whitney U test, *p<0.05, n=13–18 mice with disease per genotype; incidence: Log-rank test, ***p<0.0001, n=18–19 total mice per genotype; 2 independent experiments combined). (**c**) Representative flow plots and (**d-f**) quantification of immune cells in EAE spinal cords on day 17 after immunization (unpaired t-test; n=4 mice per genotype; **p<0.01). (**g**) Representative flow cytometry plots and (**h**,**i**) quantification of oligodendroglial cells in EAE spinal cords on day 17 after immunization

(unpaired t-test; n=3–4 mice per genotype). (**j**) Levels of IL-17A and (**k**) IFNγ from splenocytes after antigen restimulation with $MOG_{35–55}$ (Two-way ANOVA, *p=0.0184; 2 independent experiments combined).

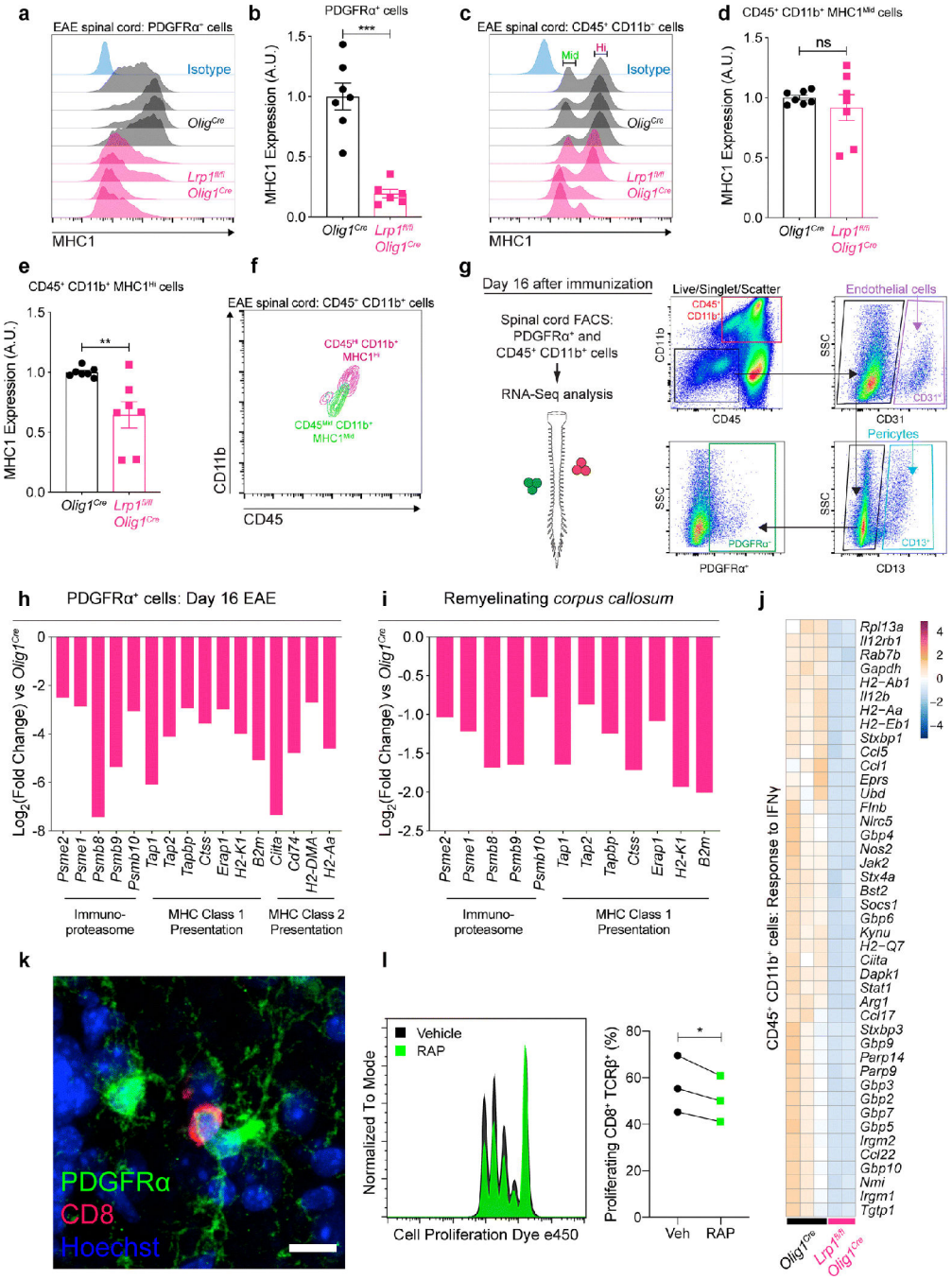

Fig. 7. LRP1 modulates MHC1-dependent antigen presentation in OPCs

(**a**) Representative histograms and **(b)** MHC1 expression in PDGFRα^{+} and **(c-e)** CD45^{+} CD11b^{+} cells from EAE spinal cords (day 17) detected by flow cytometry in *Olig1^{cre}* and *Lrp1$^{fl/fl}$Olig1^{cre}* mice (unpaired t-test, ***p<0.0001, **p=0.0076; n=6–7 mice per genotype; 2 independent experiments combined). **(f)** Backgating of MHC1 Mid (Middle) and Hi (High) expressing CD45^{+} CD11b^{+} cells in (c). **(g)** FACS gating strategy for sorting PDGFRα^{+} and CD45^{+} CD11b^{+} cells from EAE spinal cords (gates based on FMOs; CD31: endothelial cells; CD13: pericytes; SSC: side scatter area). **(h)** Antigen presentation genes

downregulated in PDGFRα$^+$ cells from *Lrp1*$^{fl/fl}$*Olig1*^{cre} EAE spinal cords. **(i)** Antigen presentation genes downregulated in the remyelinating *corpus callosum* of *Lrp1*$^{fl/fl}$*Olig1*^{cre} mice. **(j)** Genes related to IFNγ response in CD45$^+$ CD11b$^+$ cells from EAE spinal cords (GO:0034341). Heat map has a normalized count scale with z-score normalization. **(k)** OPC-CD8 cell association in the EAE spinal cord. Scale bar 10μm. **(l)** Histogram and quantification of OT-I CD8 T cell proliferation after coculture with OVA-laden OPCs in the presence or absence of RAP, an LRP1 inhibitor (n=3 independent cocultures; paired t-test, *p=0.0484).

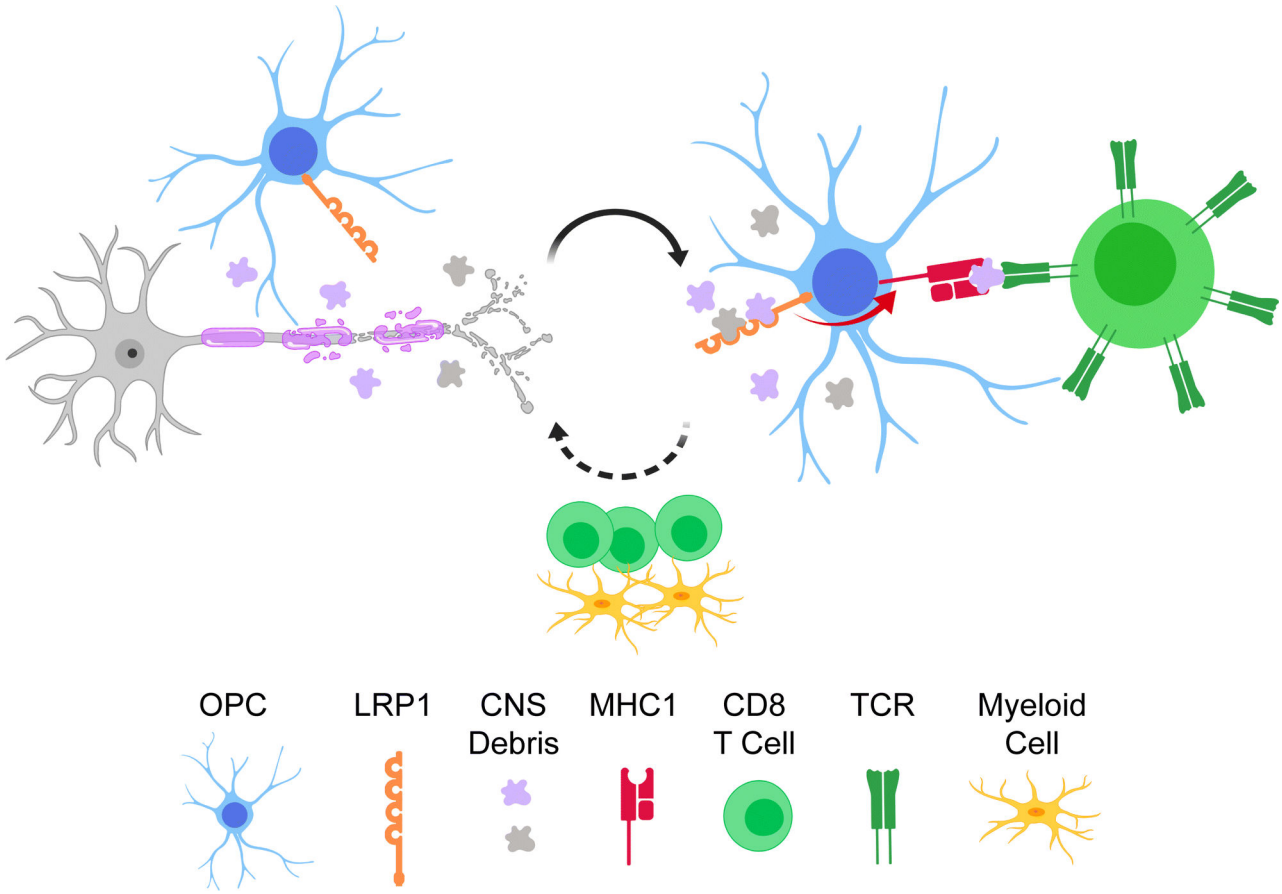

Fig. 8. Proposed model by which LRP1 in OPCs regulates the inflammatory landscape

OPCs expressing LRP1 are present in areas of CNS demyelination. LRP1 can mediate the internalization of exogenous antigen that is then processed and cross-presented via MHC1 to CD8 lymphocytes. This cross-presentation can activate CD8 effector functions, which can further exacerbate CNS pathogenesis.